Thermal effects in plasma-based accelerators*

E. Esarey,[1,2,†] C. B. Schroeder,[1] E. Michel,[2]

B. A. Shadwick,[3,1] C. G. R. Geddes,[1] and W. P. Leemans[1,2]

[1]*Lawrence Berkeley National Laboratory, Berkeley, California 94720, USA*

[2]*Department of Physics, University of Nevada, Reno, Nevada 89507, USA*

[3]*Institute for Advanced Physics, Conifer, Colorado 80433, USA*

(Dated: January 9, 2007)

Abstract

Finite plasma temperature can modify the structure of the wakefield, reduce the wavebreaking field, and lead to self-trapped electrons, which can degrade the electron bunch quality in a plasma-based accelerator. The plasma temperature evolution is described using a relativistic warm fluid theory. Alterations to the maximum amplitude of a nonlinear periodic wave exited in a plasma with nonrelativistic temperatures are presented. The trapping threshold for a plasma electron and the fraction of electrons trapped from a thermal distribution are examined using on a single-particle model. Numerical artifacts in particle-in-cell models which can mimic the physics associated with finite momentum spread are discussed.

I. INTRODUCTION

Plasma-based accelerators are capable of supporting large amplitude plasma waves with electric fields up to hundreds of GV/m, approximately three orders of magnitude beyond conventional accelerators.[1] Previously, laser-plasma accelerator experiments[2–7] have typically operated in the self-modulated regime of the laser wakefield accelerator (LWFA). In this regime, a long (compared to the plasma wavelength), high power laser pulse drives a plasma wave through a Raman or self-modulation instability. The plasma wave amplitude grows exponentially inside the laser pulse, via the instability, until the growth saturates nonlinearly or electrons become trapped in the plasma wave (subsequently damping the plasma wave due to beam loading). Experimentally, significant electron trapping is found to occur when the plasma wave amplitude surpasses a critical threshold, often loosely referred to as wavebreaking.[2,7–9] Uncontrolled trapping can result in the production of poor quality electron beams (e.g., with near 100% energy spread), which limits the application of these beams.

More recently, near-monoenergetic electron bunches have been produced in laser-plasma accelerator experiments in the 100 MeV range[8–10] as well as the 1 GeV range.[11] The source of the accelerated electrons was self-trapping from the background plasma. Narrow energy spread electron beams were produced through control of the interaction length such that the acceleration occurred over a dephasing length.[12]

To further improve the electron bunch quality and stability, a variety of laser-triggered injection methods have been proposed[13–17], and controlled injection via colliding laser pulses has been achieved experimentally.[18] The next generation of plasma accelerator experiments is likely to use a two-stage approach. The first stage would be a relatively low energy injector, wherein the accelerated electron bunch is produced through self-trapping or laser-triggered injection. The electron bunch would then be injected into the second stage, which would be a "dark current free" structure that would accelerate the bunch to high energy. A dark current free structure refers to the structure not generating any additional accelerated electrons through any self-trapping process. In order to access the viability of present and future plasma accelerator experiments, a detailed understanding and control of self-trapping is essential.

Traditionally, fluid theories have been used to define and analyze wavebreaking (the max-

imum plasma wave amplitude of a nonlinear traveling wave).[19–24] Previous hydrodynamic wavebreaking theories in one-dimension (1D) have been carried out for plasmas in the cold limit,[19] warm plasmas in the non-relativistic limit,[21] and warm plasmas in the limit of ultra-relativistic phase velocities.[22,23] The cold, relativistic wavebreaking field[19] is $\sqrt{2}(\gamma_\varphi - 1)^{1/2} E_0$, where $\gamma_\varphi^2 = 1/(1-\beta_\varphi^2)$, $v_\varphi = c\beta_\varphi$ is the plasma wave phase velocity (approximately the group velocity of the driver), $E_0 = cm\omega_p/e$, $\omega_p = ck_p = (4\pi n_0 e^2/m)^{1/2}$ is the plasma frequency, and n_0 is the ambient electron plasma density. When the plasma wave field approaches $\sqrt{2}(\gamma_\varphi - 1)^{1/2} E_0$, the cold plasma density becomes singular,[20] indicating a breakdown of the cold fluid model. In the ultra-relativistic phase velocity $\beta_\varphi = 1$ limit, the warm wavebreaking field was found[22,23] to be $E_{\rm th} \sim \theta^{-1/4} E_0$, where θ is the initial plasma temperature normalized to $mc^2/k_{\rm B}$, with $k_{\rm B}$ the Boltzmann constant. This expression for $E_{\rm th}$ is valid for $\gamma_\varphi \theta^{1/2} \gg 1$, e.g., for an ultra-relativistic ($\beta_\varphi = 1$) particle beam driver. For laser-driven plasma waves, however, typically plasma wave phase velocities are $\gamma_\varphi \sim$ 10–100 and initial plasma temperatures are $\theta mc^2 \sim 10$ eV.[25,26] Therefore, a laser-plasma accelerator typically satisfies $\gamma_\varphi \theta^{1/2} < 1$, and, hence, the above expression for $E_{\rm th}$ does not apply. Recently, a warm, relativistic fluid theory has been used to describe wavebreaking in the regime of interest to laser-plasma accelerators.[24]

For electric field amplitudes below the wavebreaking field, significant electron trapping may occur in a warm plasma. In a warm plasma, such as that characterized by a Gaussian distribution, fast electrons may exist on the tail of the distribution that can have sufficiently high momenta to allow trapping in the plasma wave. Using a test particle trapping formalism, the threshold momentum for a electron to become trapped in a plasma wave with an amplitude below the wavebreaking limit can be calculated.[27] Consequently, the fraction of electrons trapped from the tail of the distribution, which constitutes the dark current, can be determined.[27] Furthermore, the amount of trapping at the hydrodynamic warm wavebreaking limit can also be determined.

In this paper, some consequences of finite temperature on plasma-based accelerators are discussed. In Sec. II, the results of a warm, relativistic fluid model are presented. This model describes the evolution of the temperature in a plasma wakefield, as well as modification of the wakefield due to finite temperature. The warm wavebreaking limit for nonrelativistic plasma temperatures is presented. Section III discusses trapping and dark current with a test particle model. Section IV discusses numerical heating and subsequent trapping when

modeling plasma accelerators with particle-in-cell codes. Conclusions are given in Sec. V.

II. WARM WAVEBREAKING

Standard warm relativistic fluid theories derived for collisionally-dominated plasmas (e.g., Ref. 28) are inadequate for describing short-pulse laser-plasma interactions. Short-pulse laser-plasma interactions access a collisionless regime that is not in local thermodynamical equilibrium, in which the plasma electrons experience relativistic motion while the temperature (electron momentum spread) remains small. To model short-pulse laser-plasma interactions, a warm relativistic fluid model can be derived from the collisionless Boltzmann equation.[24,29] By assuming that the plasma is "warm", such that the phase-space distribution has a small momentum spread about its mean, allows the hierarchy of moment equations to be treated asymptotically.[29–33] No additional assumptions concerning the specific form of the distribution are required for closure of the fluid equations. Assuming the quasi-static approximation,[34] i.e., the plasma wave driver and fluid quantities are assumed to be functions only of the co-moving variable $\xi = z - \beta_\varphi ct$ (where z is the driver propagation direction), the fluid equations can be combined to yield the evolution equation for the nonlinear 1D plasma response[24]

$$\frac{\partial^2}{\partial \xi^2}\left[\frac{\gamma_\perp(1-\beta_\varphi w_z)}{(1-w_z^2)^{1/2}} + \frac{3}{2}\theta\frac{(1-\beta_\varphi w_z)(1-w_z^2)^{1/2}}{\gamma_\perp(1-\beta_\varphi^{-1}w_z)^2}\right] = \frac{k_p^2 w_z}{\beta_\varphi - w_z}, \tag{1}$$

where $\theta = k_B T_0/mc^2$ is the initial isotropic temperature, $\gamma_\perp^2 = 1 + a^2/2$, $a^2 \simeq 7.3 \times 10^{-19}\lambda_0^2[\mu\mathrm{m}]I_0[\mathrm{W/cm^2}]$ is the normalized laser intensity for a linear polarized laser pulse, λ_0 is the laser wavelength, and I_0 is the laser intensity. Here w_z is the axial component of the fluid velocity given by $\boldsymbol{w} = (\int d\Omega f \boldsymbol{p})/(\int d\Omega f \gamma)$, where f is the phase-space density, $\boldsymbol{p} = \gamma\boldsymbol{\beta}$ is the normalized particle momentum, and $d\Omega = d\boldsymbol{p}/\gamma$ is the invariant momentum space volume element. Linearizing Eq. (1) yields the driven wave equation $[\partial_\xi^2 + k_p^2(1 + 3\theta/2)]w_z = \partial_\xi^2 a^2$, for a plasma wave with relativistic phase velocity ($\beta_\varphi \simeq 1$). In the linear regime $a^2 \ll 1$, the dominant thermal effect is a change in the wavelength of the 1D plasma wave $\lambda \simeq \lambda_p(1 - 3\theta/4)$.

In terms of the axial fluid velocity, the plasma density is $n/n_0 = w_z/(\beta_\varphi - w_z)$, the electrostatic potential (normalized to mc^2/e) is

$$\phi = \frac{\gamma_\perp(1-\beta_\varphi w_z)}{(1-w_z^2)^{1/2}} + \frac{3}{2}\theta\frac{(1-\beta_\varphi w_z)(1-w_z^2)^{1/2}}{\gamma_\perp(1-\beta_\varphi^{-1}w_z)^2} - 1 - \frac{3}{2}\theta, \tag{2}$$

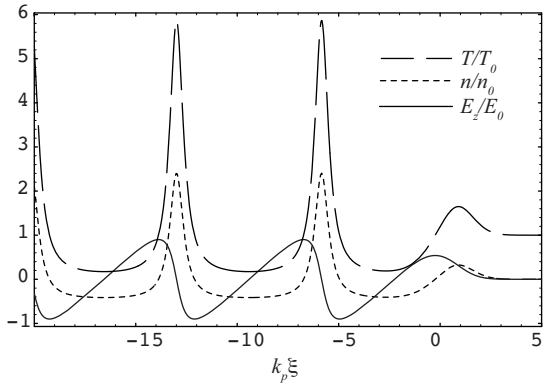

FIG. 1: Plasma density n/n_0 (dotted curve), plasma wave electric field E_z/E_0 (solid curve), and plasma temperature T/T_0 (dashed curve) excited by a Gaussian laser pulse with normalized intensity $a = 2$ and RMS length $k_p L_{\rm RMS} = 1$ (centered at $k_p\xi = 0$).

the electric field is $E_z/E_0 = -k_p^{-1}\partial_\xi\phi(w_z)$, and $k_{\rm B}T/mc^2 = (1-w_z^2)(1-\beta_\varphi^{-1}w_z)^{-2}\theta$ is the temperature [measure of thermal spread given by the contraction of the momentum variance tensor, $k_{\rm B}T/mc^2 = \mathcal{U}^\mu\mathcal{U}_\mu - 1$, with the hydrodynamic four momentum given by $\mathcal{U}^\mu = (\int d\Omega f p^\mu)/(\int d\Omega f)$].[24] The warm fluid approximation assumes $k_{\rm B}T/mc^2 < 1$ (i.e., nonrelativistic temperatures). Figure 1 shows the plasma density n/n_0 (dotted curve), plasma wave electric field E_z/E_0 (solid curve), and plasma temperature T/T_0 (dashed curve) excited by a Gaussian laser pulse $a = a_0\exp(-\xi^2/4L_{\rm RMS}^2)$ with normalized peak intensity $a_0 = 2$ and intensity RMS length $k_p L_{\rm RMS} = 1$. The plasma temperature undergoes periodic oscillations in the wake owing to compression of the plasma density.[29] Note that the temperature evolution (to lowest order in the small parameter $k_{\rm B}T/mc^2 < 1$) is given by $T = [(n/n_0)^2(1-w_z^2)]T_0$. The temperature evolution can be evaluated using the warm plasma approximation and does not require the choice of a specific distribution, as incorrectly claimed in Ref. 35.

The warm fluid model can be used to determine the maximum field amplitude $\hat{E}_{\rm max} = E_{\rm max}/E_0$ of a nonlinear periodic plasma wave with phase velocity β_φ excited in a plasma with initial temperature θ, i.e., the warm wavebreaking field,[24]

$$\hat{E}_{\rm max}^2 = \gamma_\perp\left(\chi_0 + \chi_0^{-1} - 2\right) + \left\{\frac{6\beta_\varphi^2\chi_0\left[(1-\chi_0^4) - \beta_\varphi(\chi_0^4 - 2\chi_0^2/3 + 1)\right]}{\left[(1-\beta_\varphi) - (1+\beta_\varphi)\chi_0^2\right]^3} - 1\right\}\frac{\theta}{\gamma_\perp}, \quad (3)$$

where

$$\chi_0^2 = \gamma_\varphi^2 \left(1-\beta_\varphi\right)^2 + \frac{1}{2}\gamma_\perp^{-2}(1+\beta_\varphi)^{-2}\Big\{3\beta_\varphi^2\theta + \beta_\varphi\left(48\theta\gamma_\perp^2/\gamma_\varphi^2 + 9\beta_\varphi^2\theta^2\right)^{1/2} + \Big[6\theta\beta_\varphi^2\left(10\gamma_\perp^2/\gamma_\varphi^2 + 3\beta_\varphi^2\theta\right) + 2\beta_\varphi\left(2\gamma_\perp^2/\gamma_\varphi^2 + 3\beta_\varphi^2\theta\right)\left(48\theta\gamma_\perp^2/\gamma_\varphi^2 + 9\beta_\varphi^2\theta^2\right)^{1/2}\Big]^{1/2}\Big\}. \quad (4)$$

Here $\chi_0 = (1-w_z)/(1-w_z^2)^{1/2}$ is the extrema of the fluid momenta in the co-moving frame. The maximum density perturbation is given by $(n/n_0)_{\max} = [1-\beta_\varphi^{-1}(1-\chi_0^2)/(1+\chi_0^2)]^{-1}$, which does not become singular in contrast to the cold fluid theories[19,20] (i.e., there is no shock formation). Furthermore, the absence of a singularity indicates that the fluid model remains valid, i.e., there is no break-down of the fluid model at (or before) the wavebreaking limit (contrary to the unfounded claims of Ref. 35). For wave amplitudes larger than Eq. (3), no traveling wave solutions to the fluid equations exist. At the warm hydrodynamic wavebreaking limit Eq. (3) the thermal pressure and the space charge force of the plasma wave are equal. The peak plasma temperature at the maximum plasma wave amplitude occurs at the point of maximum compression and is given by $(k_{\rm B}T/mc^2)_{\max} = 4\theta\chi_0^2[(1+\chi_0^2) - \beta_\varphi^{-1}(1-\chi_0^2)]^{-2}$. For a typical laser-plasma accelerator experiment, $\gamma_\varphi \sim 10$–100, $\gamma_\perp \sim 1$, and $\theta mc^2 \sim 10$ eV.[25,26] In this regime $\theta \ll \gamma_\perp^2/\gamma_\varphi^2 \ll 1$, and the maximum temperature to leading order is $(k_{\rm B}T/mc^2)_{\max} \simeq \gamma_\perp(\gamma_\varphi^2\theta/3)^{1/2}[1-(3\gamma_\varphi^2\theta/3)^{1/2}/(4\gamma_\perp)] \ll 1$, which confirms the validity of the warm plasma approximation at the maximum plasma wave amplitude.

The warm fluid theory used above is an approximation based on an asymptotic perturbation expansion assuming small thermal spread and does not require specific assumptions about the initial plasma distribution. If the temperature becomes relativistic this expansion will no longer be valid. For relativistic temperatures, the higher-order moments of the distribution will be important and will be a function of the specific form of the phase-space distribution. Note that choice of an unphysical distribution (e.g., water-bag) may lead to singular (unbounded) solutions. These singularities are not physical (as erroneously speculated in Ref. 35), but the result of the choice of an unphysical phase-space distribution. It should also be noted that for sufficiently large (or singular) density the collisionless plasma model will no longer be valid.

In the cold plasma limit ($\theta = 0$), Eq. (3) reduces to $\hat{E}_{\max}^2(\theta=0) = 2\gamma_\perp\left(\gamma_\varphi - 1\right)$. This is a

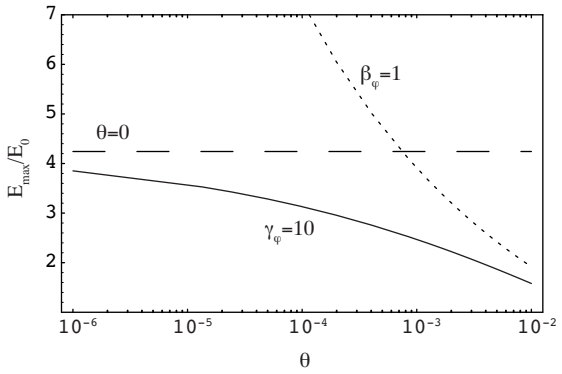

FIG. 2: Maximum plasma wave electric field amplitude $\hat{E}_{\rm max} = E_{\rm max}/E_0$ [Eq. (3)] versus initial temperature θ with $\gamma_\varphi = 10$ and $\gamma_\perp = 1$. The dotted curve is the ultra-relativistic result $\beta_\varphi = 1$, and the dashed line is the cold limit.

generalization[24,27] of the cold relativistic wavebreaking field[19,36] to include the presence of a laser field. In the regime relevant to laser-plasma accelerator experiments, $\theta \ll \gamma_\perp^2/\gamma_\varphi^2 \ll 1$, Eq. (3) reduces to[24]

$$\hat{E}_{\rm max}^2 \simeq 2\gamma_\perp(\gamma_\varphi - 1) - \gamma_\varphi \left[\frac{8}{3}\left(3\gamma_\varphi^2\gamma_\perp^2\theta\right)^{1/4} - 2\left(3\gamma_\varphi^2\theta\right)^{1/2}\right]. \tag{5}$$

Equation (5) is the cold relativistic wavebreaking field with the lowest order reduction due to the plasma temperature. For high-intensity lasers ($a^2 \gtrsim 1$), Eq. (5) indicates that $E_{\rm max}$ inside a laser pulse is significantly larger compared to behind the pulse (where $a = 0$).[24]

Figure 2 shows the wavebreaking field Eq. (3), $\hat{E}_{\rm max} = E_{\rm max}/E_0$ (solid curve), versus initial temperature θ with $\gamma_\varphi = 10$ and $\gamma_\perp = 1$. The dotted curve is the ultra-relativistic result ($\beta_\varphi = 1$), and the dashed line is the cold limit ($\theta = 0$). Note that for typical short-pulse laser-plasma-interactions, $\theta \sim 10^{-4}$. Figure 3(a) shows the maximum density perturbation calculated by solving Eq. (1) assuming a drive laser pulse pulse with a Gaussian longitudinal profile $a = a_0 \exp(-\xi^2/4L_{\rm RMS}^2)$ with RMS intensity pulse length of $k_p L_{\rm RMS} = 1$ propagating in a plasma with density such that $\gamma_\varphi = 10$. As the amplitude approaches the wavebreaking limit $(\delta n/n_0)_{\rm max} = [1 - \beta_\varphi^{-1}(1-\chi_0^2)/(1+\chi_0^2)]^{-1} - 1$ (dotted line), the peak density perturbation is modified from the cold result. Figure 3(b) shows the difference between the nonlinear plasma wavelengths $(\Delta\lambda/\lambda_p)/\theta = [\lambda(\theta=0) - \lambda]/(\theta\lambda_p)$ (solid curve), the peak electric fields $(\Delta E/E_0)/\theta = [E_z(\theta=0) - E_z]/(\theta E_0)$ (dotted curve), and the peak electrostatic potentials $\Delta\phi/\theta = [\phi(\theta=0) - \phi]/\theta$ (dashed curve), assuming an initially cold ($\theta = 0$) and warm ($\theta = 10^{-3}$) plasma versus drive laser amplitude a_0 (with $k_p L_{\rm RMS} = 1$

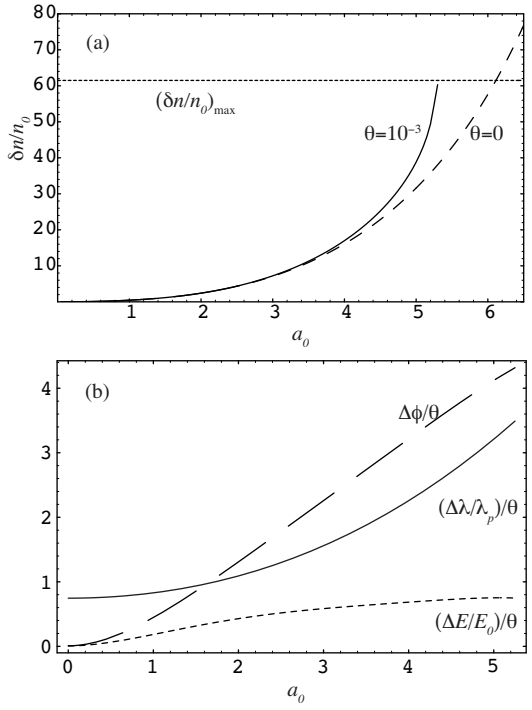

FIG. 3: (a) Peak density perturbation versus amplitude of drive laser a_0 (with $k_p L_{\rm RMS} = 1$ and $\gamma_\varphi = 10$) for initial plasma temperature of $\theta = 10^{-3}$ (solid curve) and $\theta = 0$ (dashed curve). Dotted line in (a) is the wavebreaking limit $(n/n_0)_{\max} - 1$ behind the drive laser for $\gamma_\varphi = 10$ and $\theta = 10^{-3}$. (b) Difference between the nonlinear plasma wavelengths $(\Delta\lambda/\lambda_p/\theta)$ (solid curve), difference between the peak electric field amplitudes $(\Delta E/E_0)/\theta$ (dotted curve), and difference between the peak potential amplitudes $\Delta\phi/\theta$ (dashed curve), assuming an initially cold ($\theta = 0$) and warm ($\theta = 10^{-3}$) plasma versus drive laser amplitude a_0.

and $\gamma_\varphi = 10$). Note that the differences plotted in Fig. 3(b) are normalized to θ. As Fig. 3(b) indicates, the normalized potential and electric field of the wave in a warm plasma differ from the cold result by a factor of order $\sim \theta \ll 1$ (typically $\theta \sim 10^{-4}$), and below wavebreaking, the electric field is well-modelled by the cold plasma result for nonrelativistic initial temperatures.[29] This is in contrast to the mistaken claims of Ref. 35 that the cold plasma response can not be used to approximately model the electrostatic field of a plasma wave below wavebreaking. For $a_0 \ll 1$, $[\lambda(\theta = 0) - \lambda]/(\theta\lambda_p) = 3/4$ (the 1D relativistic Bohm-Gross thermal shift in the plasma wavelength), as shown in Fig. 3(b).

III. PARTICLE TRAPPING

The dynamics of an electron in the presence of a plasma wave and a laser pulse is determined by the Hamiltonian in the co-moving frame[37] $H = (\gamma_\perp^2 + u^2)^{1/2} - \beta_\varphi u - \phi(\xi)$, where u is the electron momentum normalized to mc. Assuming the quasi-static approximation, the Hamiltonian is time independent and, therefore, a constant of motion $H(u, \xi) = \text{constant}$. The electron momentum at any phase is

$$u = \beta_\varphi \gamma_\varphi^2 \left(H + \phi\right) \pm \gamma_\varphi \left[\gamma_\varphi^2 \left(H + \phi\right)^2 - \gamma_\perp^2\right]^{1/2}. \tag{6}$$

Equation (6) describes trapped (closed) and untrapped (open) orbits, in which a particular orbit is specified by a particular value of $H = \text{constant}$. The separatrix orbit between trapped and untrapped orbits is given by $H = H_s$, where $H_s = \gamma_\perp(\xi_m)/\gamma_\varphi - \phi(\xi_m)$. Here, ξ_m is the phase that maximizes $H(\gamma_\perp(\xi)\gamma_\varphi\beta_\varphi, \xi)$. Assuming $\gamma_\perp = \text{constant}$, $\phi(\xi_m) = \phi_{\min}$ is the minimum potential of the plasma wave.

Consider a plasma electron with initial normalized momentum u_t in the absence of any fields (i.e., before the passage of the driver and excitation of the plasma wave, $\gamma_\perp = 1$ and $\phi = 0$). The orbit of the electron will be defined by the Hamiltonian $H = H_t$, where $H_t = (1 + u_t^2)^{1/2} - \beta_\varphi u_t$. Trapping of the electron will occur when the orbit defined by the Hamiltonian H_t coincides with a trapped orbit, defined by the separatrix orbit, namely, when $H_t \leq H_s$. For $H_t > H_s$, the electron is on an untrapped orbit. Solving $H_t = H_s$ yields in the minimum initial electron momentum for trapping in the plasma wave,[27]

$$u_t = \gamma_\varphi\beta_\varphi \left(\gamma_\perp - \gamma_\varphi\phi_{\min}\right) - \gamma_\varphi \left[\left(\gamma_\perp - \gamma_\varphi\phi_{\min}\right)^2 - 1\right]^{1/2}. \tag{7}$$

Equation (7) is valid for a plasma wave potential in a *warm* plasma, where $\phi_{\min}$ is the extrema of the plasma wave potential [solution of Eq. (1)]. Figure 4 shows the initial momentum u_t required for the electron to be trapped by a plasma wave with amplitude $\hat{E}_m = E_{\text{peak}}/E_0$, with$\gamma_\perp = 1$. In Fig. 4 the peak electric field corresponding to the minimum potential $\phi_{\min}(\hat{E}_m)$ was solved using Eq. (1) for a warm plasma with $\theta = 10^{-4}$. The threshold momentum required for trapping decreases for larger plasma wave amplitude and for lower plasma wave phase velocity. Note that trapping can occur for plasma waves with ultra-relativistic phase velocities ($\beta_\varphi = 1$); with $\beta_\varphi = 1$ and $\gamma_\perp = 1$, Eq. (7) reduces to $u_t = (\phi_{\min} - 1/\phi_{\min})/2$.

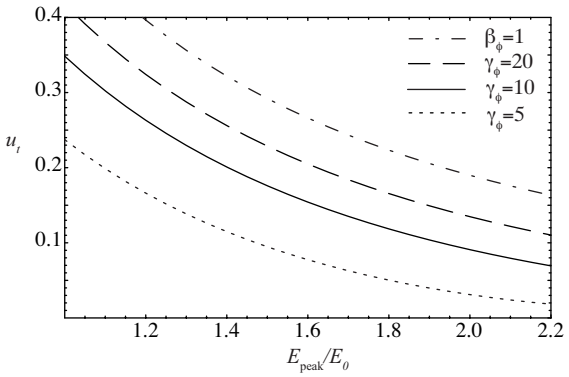

FIG. 4: Initial electron momentum u_t required to be trapped by a plasma wave with field amplitude $E_{\rm peak}/E_0$ and phase velocity $\gamma_\varphi = 5$ (dotted curve), $\gamma_\varphi = 10$ (solid curve), $\gamma_\varphi = 20$ (dashed curve), and $\beta_\varphi = 1$ (dash-dotted curve), assuming an initial plasma temperature $\theta = 10^{-4}$.

As shown in Fig. 3 (and Ref. 33) the fields are weakly influenced by the width of the distribution, $E_{\rm peak}(\theta)/E_0 - E_{\rm peak}(\theta = 0)/E_0 \sim \theta$, below the wavebreaking limit. Thus, contrary to the unfounded conjecture in Ref. 35, it is an excellent approximation to use the cold fields when studying a warm plasma for typical laser-plasma accelerator parameters. For a cold plasma, the relation between the minimum potential and the field amplitude is

$$\phi_{\rm min} = \gamma_\perp - 1 + \hat{E}_m^2/2 - \beta_\varphi \left[\left(\gamma_\perp + \hat{E}_m^2/2 \right)^2 - \gamma_\perp^2 \right]^{1/2}, \tag{8}$$

where $\hat{E}_m = E_{\rm peak}/E_0$ is the normalized amplitude of the plasma wave field. Equations (7) and (8) can be solved for the peak field E_t required for the onset of particle trapping as a function of the initial electron momentum u_t,[27]

$$(E_t/E_0)^2 \simeq 2\gamma_\perp (\gamma_\varphi - 1) + 2\gamma_\varphi^2 \beta_\varphi \left\{ u_t - \left[(\beta_\varphi u_t)^2 + 2\beta_\varphi u_t \gamma_\perp/\gamma_\varphi \right]^{1/2} \right\}, \tag{9}$$

where $u_t \ll 1$ (non-relativistic initial momentum) has been assumed.

Note that trapping occurs in a warm plasma in the ultra-relativistic phase velocity limit where the wave phase velocity is equal to the speed of light $v_\varphi = c$ (as shown in Fig. 4). For $\gamma_\perp = 1$, $\beta_\varphi = 1$, and $u_t \ll 1$, Eq. (7) yields $\phi_{\rm min} \simeq -1 + u_t$, and, using Eq. (8), the peak field of an ultra-relativistic plasma wave required for trapping an electron with initial momentum u_t is $E_t/E_0 \simeq u_t^{-1/2}$. This result refutes the incorrect claim of Ref. 35 that trapping can not occur for plasma waves with $\beta_\varphi = 1$. Indeed, with $\beta_\varphi = 1$, the separatrix between trapped and untrapped particles is finite for all phases except ξ_m (which is never reached by a trapped particle).

Equation (7) concerns the trapping in a plasma wave of a single plasma electron with initial momentum u_t. For a thermal plasma electron distribution, electrons on the tail of the distribution function may have sufficiently high momentum so as to reside on trapped orbits. The fraction of electrons trapped in the plasma wave can be computed for a given initial momentum distribution. For example, assuming an initial Gaussian momentum distribution of the plasma electrons with initial temperature T_0 defined by the RMS momentum spread $(k_{\rm B}T_0/m_e)^{1/2}$, with $(k_{\rm B}T_0/m_ec^2)^{1/2} \ll 1$ [i.e., a momentum distribution of the form $F(u) \propto \exp(-u^2/2\theta)$], the fraction of trapped electrons is[27]

$$f_{\rm trap} = \frac{1}{2}{\rm erfc}\left(u_t/\sqrt{2\theta}\right), \tag{10}$$

where u_t is given by Eq. (7). Note that only electrons with momenta in the direction of the phase velocity of the plasma wave are trapped.

Figure 5 shows the fraction of trapped electrons versus the initial temperature of a Gaussian plasma electron momentum distribution for three different nonlinear plasma wave amplitudes driven by a laser with $k_pL_{\rm RMS} = 1$ and $a_0 = 3.65$ ($\hat{E}_m \simeq 1.75$), $a_0 = 4.15$ ($\hat{E}_m \simeq 2$), and $a_0 = 4.75$ ($\hat{E}_m \simeq 2.25$), with $\gamma_\varphi = 10$. Note that the plasma wave was calculated assuming a *warm* plasma with temperature θ via Eq. (1). The total number of trapped electrons (i.e., dark current in the plasma accelerator) can be estimated from Eq. (10). For example, for a plasma density of $n_0 = 10^{19}$ cm^{-3}, driver transverse size of $r_\perp = 10$ μm, and accelerator length of 1 mm, a trapping fraction of $f_{\rm trap} = 10^{-3}$ indicates ~ 0.1 nC of trapped charge. This trapping calculation neglects beam loading, which implies the wakefield induced by the trapped electrons is much smaller than the primary plasma wave, or $n_{\rm trap}/n_0 \ll |\phi|$, where $n_{\rm trap}$ is the density of the trapped electron bunch.

As the driver propagates into the plasma, more charge will be trapped until the amplitude of the plasma wave is substantially reduced due to beam loading. The beam loading limit is defined as the number of accelerated electrons required to produce a wakefield that cancels the accelerating field of the plasma wave.[38] The trapped bunch density is approximately given by $n_b \simeq f_{\rm trap}n_0z/L_b$, where z is the propagation distance and L_b is the bunch length. Assuming $k_pL_b \lesssim 1$, the wakefield generated by the bunch is given by $E_b/E_0 \simeq k_pL_bn_b/n_0$ in the 1D limit, assuming $E_b/E_0 < 1$. The beam loading limit at which $E_b \simeq E_m$ is then reached after a propagation distance of $z_{\rm BL} \approx k_p^{-1}f_{\rm trap}^{-1}\hat{E}_m$. For $\hat{E}_m \sim 1$ and $f_{\rm trap} \ll 1$, $k_pz_{\rm BL} \gg 1$ and beam loading will only be significant after long propagation distances.

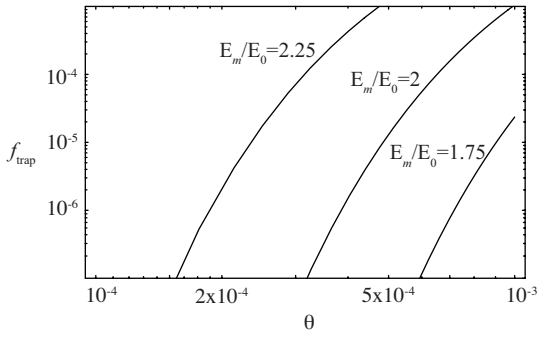

FIG. 5: Fraction of trapped electrons $f_{\rm trap}$ [Eq. (10)] versus the initial temperature of a Gaussian plasma electron distribution $\theta = k_{\rm B}T_0/mc^2$ for three different nonlinear plasma wave amplitudes driven by a laser with $k_pL_{\rm RMS} = 1$ and $a_0 = 3.65$ ($\hat{E}_m \simeq 1.75$), $a_0 = 4.15$ ($\hat{E}_m \simeq 2$), and $a_0 = 4.75$ ($\hat{E}_m \simeq 2.25$), with $\gamma_\varphi = 10$.

For a given initial plasma temperature and plasma wave phase velocity, a larger fraction of electrons become trapped as the plasma wave amplitude increases. The particle trapping model presented in this section, can be used to calculate the fraction trapped at the hydrodynamic wavebreaking field. For simplicity, consider $\gamma_\perp = 1$. Equation (7) can be solved for the plasma wave potential required for trapping an electron with initial momentum u_t, $\phi_{\rm min} = \gamma_\varphi^{-1} - (1 + u_t^2)^{1/2} + \beta_\varphi u_t \simeq \gamma_\varphi^{-1} - 1 + \beta_\varphi u_t$, for $u_t \ll 1$. The minimum potential at the wavebreaking amplitude is given by Eq. (2) with $w_z = (1 - \chi_0^2)/(1 + \chi_0^2)$, where χ_0 is given by Eq. (4). Assuming $\theta \ll 1$, yields $\phi_{\rm WB} \simeq \gamma_\varphi^{-1} - 1 + \beta_\varphi\sqrt{3\theta}$. Hence, at the wavebreaking amplitude, a significant fraction of the plasma electrons (satisfying $u_t > \sqrt{3\theta}$) will be trapped: $f_{\rm trap} = {\rm erfc}(\sqrt{3/2})/2 \simeq 0.04$. Note that here we have used the potential derived from the *warm* fluid equations. This shows that significant trapping occurs below the wavebreaking limit for a physical initial electron distribution (e.g., Gaussian) and refutes the incorrect claims[35] that there is no trapping below the wavebreaking limit.

The warm fluid theory of wavebreaking and the trapping calculation assume the quasi-static approximation that the plasma wave is a function of only $\xi = z - v_\varphi t$. In general, for the plasma wave to be a traveling wave that is a function of only ξ implies that there is sufficiently small trapping and beam loading such that any time dependent damping of the plasma wave is insignificant (i.e., $k_p z_{\rm BL} \gg 1$, as discussed above). At the wavebreaking amplitude, the fraction trapped is $f_{\rm trap} \simeq 4\%$ assuming an initial Gaussian electron momentum distribution. For example, if the beam loading estimate discussed above is assumed to

approximately apply in the nonlinear limit, then $f_{\rm trap} \simeq 4\%$ and $\hat{E}_{\rm WB} \simeq 3$ imply $z_{\rm BL} \simeq 12\lambda_p$. This simple estimation implies that beam loading can lead to appreciable reduction of the plasma wave after several plasma periods if the field amplitude approaches the hydrodynamic wavebreaking limit.

IV. MODELING WITH PARTICLE-IN-CELL CODES

Particle-in-cell (PIC) codes[39–41] have been used extensively to model laser-plasma-based accelerator experiments. In a particle-grid approach such as PIC, finite-sized, charged macro-particles interact with electromagnetic fields defined on a grid and interpolated to the macro-particle positions. The unavoidable discretization of the physical model and the small number of macro-particles used to represent the phase space distribution both give rise to unphysical heating.[40,41] These heating mechanisms include scattering[42] and grid heating.[43] Numerical heating via scattering has a continuous slow growth of momentum spread is due to the finite number of macro-particles. The growth of momentum spread depends mainly on the number of macro-particles per cell and on the particle shape. Grid heating[43] has a fast growth rate and saturates when $\lambda_{\rm D} \sim \Delta z$ in 1D, where $\lambda_{\rm D} = (k_{\rm B}T/4\pi ne^2)^{1/2}$ is the Debye length and Δz the grid size. Interpolation of the gridded field quantities to the macro-particle positions leads to numerical errors in the trajectories that appear to be qualitatively different than the trajectory errors due to truncation in the particle integrator. These numerical errors will alter the macro-particle phase space and can mimic physical processes leading to the incorrect interpretation of computational results. This will be of particular importance when attempting to model detailed kinetic effects, such as trapping of the background electrons or generation of dark current in a plasma-based accelerator.

The effect of the unphysical heating (macro-particle momentum spread) in PIC codes is studied for the case of a nonlinear plasma wave driven by a short laser pulse.[44] For the study described in this section, the initial normalized laser intensity profile is of the form $a_0^2 \exp(-2z^2/L^2)$ with $a_0 = 2$, $k_pL = 2$, and $\omega_0/\omega_p = 10$. For a 0.8-μm laser wavelength, the plasma wavelength is 8 μm (plasma number density of 1.7×10^{19} cm^{-3}), $L = 2.5$ μm (10 fs FWHM laser intensity duration), and peak laser intensity of 8.5×10^{18} W/cm^2. The 1D simulation box is 130 μm long, and the laser was launched from the boundary of the simulation box. The number of grid points varies according to the resolution. The macro-

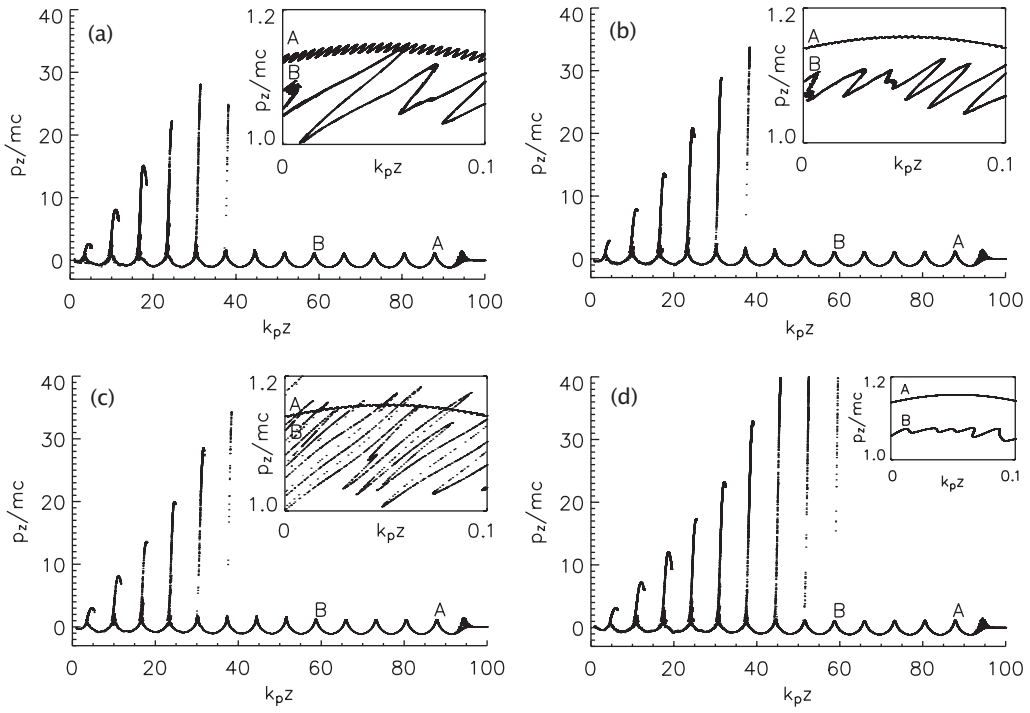

FIG. 6: Macro-particle phase space at $t = 15.75\lambda_p/c$, with the physical parameters $\omega_0/\omega_p = 10$, $a_0 = 2$, and $k_pL = 2$, using the numerical parameters: (a) $\Delta z = \lambda_0/36$ and $N_{\rm ppc} = 400$, (b) $\Delta z = \lambda_0/48$ and $N_{\rm ppc} = 400$, (c) $\Delta z = \lambda_0/48$ and $N_{\rm ppc} = 100$, and (d) $\Delta z = \lambda_0/48$ and $N_{\rm ppc} = 400$ with a filter[47] on the current. The insets show a magnification of the phase-space at the first (A) and fifth (B) buckets after the laser pulse.

particles are loaded uniformly and cold (no initial momentum), using either $N_{\rm ppc} = 100$ or $N_{\rm ppc} = 400$, where $N_{\rm ppc}$ is the number of macro-particles per cell. For the simulations, a modified version of Plasma Simulation Code (PSC)[45] is used, which implements the standard PIC algorithm[40] and uses a charge-conserving current-deposition scheme.[46]

For this case we expect no self-trapping in the wake because the plasma is initially cold and the wakefield is below the cold relativistic wavebreaking field, $E_z < E_0[2(\gamma_\varphi - 1)]^{1/2}$. The evolution of the plasma temperature should follow the warm fluid model,[29,33] which predicts that an initially cold collisionless plasma remains cold in this regime. However, the PIC simulations show macro-particles trapped in the wake, as seen in Fig. 6. Figure 6 shows the macro-particle phase space (momentum versus position) at $t = 15.75\lambda_p/c$ for the numerical parameters: (a) $\Delta z = \lambda_0/36$ and $N_{\rm ppc} = 400$, (b) $\Delta z = \lambda_0/48$ and $N_{\rm ppc} = 400$, (c) $\Delta z = \lambda_0/48$ and $N_{\rm ppc} = 100$, and (d) $\Delta z = \lambda_0/48$ and $N_{\rm ppc} = 400$ with a (1,2,1)

filter (including compensator)[47] on the current. The insets show a magnification of the phase-space at the first (A) and fifth (B) buckets after the laser pulse. Note that the wake amplitude is lower in the fifth bucket compared to the first. This is due to the laser evolution (self-steepening of the laser pulse) resulting in a higher peak laser intensity as the laser propagates through the plasma (this has also been confirmed by comparison with 1D cold fluid simulations of the same physical parameters). The insets of Fig. 6 show that, as a function of distance behind the driver, phase space develops an increasingly complex structure. When the plasma current is deposited on the grid, this course graining will yield a current which will have characteristics similar to that due to a warm distribution. In particular this course graining will trigger grid heating, leading to an increasingly large momentum spread. As shown in Figs. 6(a)–(c), the phase space structure is dependent on the resolution and number of macro-particles per cell. At a resolution of $\Delta z = \lambda_0/36$ the longitudinal electric field is accurately represented. Increasing the resolution leads to very little change in the wakefield, but results in significant changes in the macro-particle phase space. Note that for a warm initial condition, the PIC algorithm has been shown, with sufficient resolution and macro-particles per cell, to yield the correct thermal plasma response.[33]

The longitudinal mean square macro-particle momentum spread, $\sigma_u^2 = \langle (u - \langle u \rangle)^2 \rangle$, is shown in Fig. 7. In this example, secular growth of the momentum spread occurs after the third plasma wave bucket. Increasing longitudinal resolution reduces the momentum spread; Fig. 7(a) shows resolutions of $\Delta z = \lambda_0/60$ (red curve) and $\Delta z = \lambda_0/36$ (black curve). Increasing the macro-particles per cell also reduces the momentum spread; Fig. 7(b) shows $N_{\rm ppc} = 100$ (red curve) and $N_{\rm ppc} = 400$ (black curve).

V. SUMMARY AND DISCUSSION

The performance of plasma-based accelerators can be affected by finite plasma temperature. Finite temperatures reduce the wavebreaking field and enhance the amount of self-trapped electrons thus leading to the production of dark current, which will degrade the accelerated electron bunch quality. To correctly determine the temperature evolution, a warm relativistic fluid theory has been derived and analyzed.[29,33] The plasma temperature is found to undergo periodic oscillations in the wake, due to adiabatic compression, but

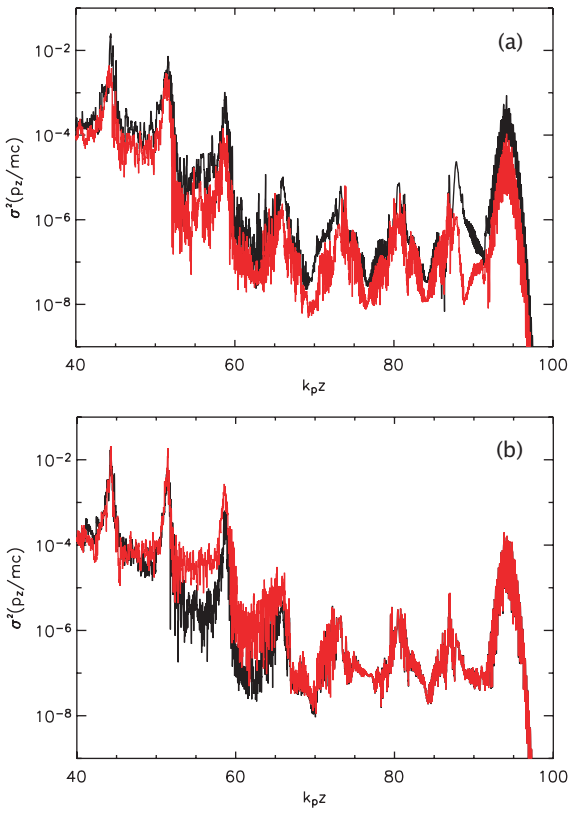

FIG. 7: (a) Normalized mean square momentum spread calculated in each cell for $\Delta z = \lambda_0/36$ and $N_{\rm ppc} = 400$ (black curve) and $\Delta z = \lambda_0/60$ and $N_{\rm ppc} = 400$ (red curve). (b) Normalized mean square momentum spread calculated in each cell for $\Delta z = \lambda_0/48$ and $N_{\rm ppc} = 400$ (black curve) and $\Delta z = \lambda_0/48$ and $N_{\rm ppc} = 100$ (red curve). The physical parameters are $\omega_0/\omega_p = 10$, $a_0 = 2$, and $k_pL = 2$.

there is no secular heating.[29,33] This is the case since, in the underdense regime of plasma accelerators, there are no collisions, and, in the standard wakefield case, the plasma response is well-described using the quasi-static approximation. Using a warm fluid model, an analytical result for the maximum field amplitude of a periodic nonlinear plasma wave (warm wavebreaking limit) was derived.[24] The warm wavebreaking limit Eq. (3) is capable of describing the regime of current ultra-intense short-pulse laser interactions with underdense plasma, in contrast to previous results that are limited to ultra-relativistic particle drive beams. This field amplitude is a fundamental limit on the accelerating gradient in plasma-based accelerators.

For wake amplitudes below the wavebreaking limit, fast particles on the tail of a thermal

distribution may become trapped. The trapping of thermal plasma electrons in a nonlinear plasma wave has been examined using a formalism based on single-particle dynamics and the threshold electric field amplitude for trapping an electron with arbitrary momentum in a nonlinear plasma wave was derived.[27] This calculation included the presence of a laser field, which was found to increase the trapping threshold and, hence, reduce the fraction of trapped electrons. The dark current, or the fraction of electrons trapped, was calculated as a function of initial plasma temperature, wave amplitude, and wave phase velocity.[27]

Several numerical effects in PIC codes can lead to phase space errors, unphysical heating of the model plasma (i.e., an unphysically large macro-particle momentum spread), and erroneously large levels of particle trapping. Since numerical heating increases with distance behind the wake driver, this issue is worse for larger simulation boxes. For the examples presented in Sec. IV, numerical trapping was observed to occur behind the seventh period of the wake when $a_0 = 2$. For $a_0 = 3$, however, numerical trapping occurred after the first three wake periods. Care must be taken in choosing the numerical parameters to ensure that artificial numerical effects are sufficiently small. Although the results presented in this paper have been limited to 1D, this same general behavior is observed to occur in 2D PIC simulations.[44,48] Further studies indicate that the use of shaped macro-particles may reduce these effects, however, numerical heating and unphysical trapping will still occur.[48]

ACKNOWLEDGMENTS

The authors would like to thank Hartmut Ruhl for kindly providing the PIC code PSC and for related discussions. This work was supported by the Director, Office of Science, Office of High energy Physics, of the U.S. Department of Energy under contract DE-AC02-05CH11231, by the University of Nevada, Reno, grant DE-FC52-01NV14050, and by a Scientific Discovery through Advanced Computing project, "Advanced Computing for 21st Century Accelerator Science and Technology," which is supported by the U.S. DOE/SC Office of High Energy Physics and the Office of Advanced Scientific Computing Research. Computational resources were provided by an INCITE grant. This research used resources

of the National Energy Research Scientific Computing Center.

---

* Paper UI2 3, Bull. Am. Phys. Soc. **51**, (2006).

† Invited speaker.

[1] E. Esarey, P. Sprangle, J. Krall, and A. Ting, IEEE Trans. Plasma Sci. **24**, 252 (1996).

[2] A. Modena, Z. Najmudin, A. E. Dangor, C. E. Clayton, K. A. Marsh, C. Joshi, V. Malka, C. B. Darrow, C. Danson, D. Neely, *et al.*, Nature **377**, 606 (1995).

[3] R. Wagner, S.-Y. Chen, A. Maksimchuk, and D. Umstadter, Phys. Rev. Lett. **78**, 3125 (1997).

[4] A. Ting, C. I. Moore, K. Krushelnick, C. Manka, E. Esarey, P. Sprangle, R. Hubbard, H. R. Burris, R. Fischer, and M. Baine, Phys. Plasmas **4**, 1889 (1997).

[5] C. Gahn, G. D. Tsakiris, A. Pukhov, J. Meyer-ter-Vehn, G. Pretzler, P. Thirolf, D. Habs, and K. J. Witte, Phys. Rev. Lett. **83**, 4772 (1999).

[6] W. P. Leemans, P. Catravas, E. Esarey, C. G. R. Geddes, C. Toth, R. Trines, C. B. Schroeder, B. A. Shadwick, J. van Tilborg, and J. Faure, Phys. Rev. Lett. **89**, 174802 (2002).

[7] V. Malka, S. Fritzler, E. Lefebvre, M.-M. Aleonard, F. Burgy, J.-P. Chambaret, J.-F. Chemin, K. Krushelnick, G. Malka, S. P. D. Mangles, *et al.*, Science **298**, 1596 (2002).

[8] S. P. D. Mangles, C. D. Murphy, Z. Najmudin, A. G. R. Thomas, J. L. Collier, A. E. Dangor, E. J. Divall, P. S. Foster, J. G. Gallacher, C. J. Hooker, *et al.*, Nature **431**, 535 (2004).

[9] J. Faure, Y. Glinec, A. Pukhov, S. Kiselev, S. Gordienko, E. Lefebvre, J.-P. Rousseau, F. Burgy, and V. Malka, Nature **431**, 541 (2004).

[10] C. G. R. Geddes, C. Toth, J. van Tilborg, E. Esarey, C. B. Schroeder, D. Bruhwiler, C. Nieter, J. Cary, and W. P. Leemans, Nature **431**, 538 (2004).

[11] W. P. Leemans, B. Nagler, A. J. Gonsalves, C. Tóth, K. Nakamura, C. G. R. Geddes, E. Esarey, C. B. Schroeder, and S. M. Hooker, Nature Phys. **2**, 696 (2006).

[12] C. G. R. Geddes, C. Tóth, J. van Tilborg, E. Esarey, C. B. Schroeder, D. Bruhwiler, C. Nieter, J. Cary, and W. P. Leemans, Phys. Plasmas **12**, 056709 (2005).

[13] D. Umstadter, J. K. Kim, and E. Dodd, Phys. Rev. Lett. **76**, 2073 (1996).

[14] E. Esarey, R. F. Hubbard, W. P. Leemans, A. Ting, and P. Sprangle, Phys. Rev. Lett. **79**, 2682 (1997).

[15] C. B. Schroeder, P. B. Lee, J. S. Wurtele, E. Esarey, and W. P. Leemans, Phys. Rev. E **59**,

6037 (1999).

[16] G. Fubiani, E. Esarey, C. B. Schroeder, and W. P. Leemans, Phys. Rev. E **70**, 016402 (2004).

[17] H. Kotaki, S. Masuda, M. Kando, J. K. Koga, and K. Nakajima, Phys. Plasmas **11**, 3296 (2004).

[18] J. Faure, C. Rechatin, A. Norlin, A. Lifschitz, Y. Glinec, and V. Malka, Nature **444**, 737 (2006).

[19] A. I. Akhiezer and R. V. Polovin, Zh. Eksp. Teor. Fiz. **30**, 915 (1956), [Sov. Phys. JEPT **3**, 696 (1956)].

[20] J. M. Dawson, Phys. Rev. **113**, 383 (1959).

[21] T. P. Coffey, Phys. Fluids **14**, 1402 (1971).

[22] T. Katsouleas and W. B. Mori, Phys. Rev. Lett. **61**, 90 (1988).

[23] J. B. Rosenzweig, Phys. Rev. A **38**, 3634 (1988).

[24] C. B. Schroeder, E. Esarey, and B. A. Shadwick, Phys. Rev. E **72**, 055401 (2005).

[25] C. G. Durfee III, J. Lynch, and H. M. Milchberg, Phys. Rev. E **51**, 2368 (1995).

[26] P. Volfbeyn, E. Esarey, and W. Leemans, Phys. Plasmas **6**, 2269 (1999).

[27] C. B. Schroeder, E. Esarey, B. A. Shadwick, and W. P. Leemans, Phys. Plasmas **13**, 033103 (2006).

[28] S. R. de Groot, W. A. van Leeuwen, and C. G. van Weert, *Relativistic Kinetic Theory* (North-Holland, Amsterdam, 1980).

[29] B. A. Shadwick, G. M. Tarkenton, and E. H. Esarey, Phys. Rev. Lett. **93**, 175002 (2004).

[30] W. A. Newcomb, Phys. Fluids **25**, 846 (1982).

[31] P. Amendt, Phys. Fluids **29**, 1458 (1986).

[32] J. G. Siambis, Phys. Fluids **30**, 896 (1986).

[33] B. A. Shadwick, G. M. Tarkenton, E. H. Esarey, and C. B. Schroeder, Phys. Plasmas **12**, 056710 (2005).

[34] P. Sprangle, E. Esarey, and A. Ting, Phys. Rev. Lett. **64**, 2011 (1990).

[35] R. M. G. M. Trines and P. A. Norreys, Phys. Plasmas **13**, 123102 (2006).

[36] E. Esarey, C. B. Schroeder, W. P. Leemans, and B. Hafizi, Phys. Plasmas **6**, 2262 (1999).

[37] E. Esarey and M. Pilloff, Phys. Plasmas **2**, 1432 (1995).

[38] T. Katsouleas, S. Wilks, P. Chen, J. M. Dawson, and J. J. Su, Part. Accel. **22**, 81 (1987).

[39] J. M. Dawson, Rev. Mod. Phys. **55**, 403 (1983).

[40] C. K. Birdsall, A. B. Langdon, V. Vehedi, and J. P. Verboncoeur, *Plasma Physics via Computer Simulations* (Adam Hilger, Bristol, Eng., 1991).

[41] R. Hockney and J. Eastwood, *Computer Simulation using Particles* (Taylor & Francis Group, New York, 1988).

[42] R. W. Hockney, J. Comp. Phys. **8**, 19 (1971).

[43] A. B. Langdon, J. Comp. Phys. **6**, 247 (1970).

[44] E. Michel, B. A. Shadwick, C. B. Schroeder, C. G. R. Geddes, E. Esarey, W. P. Leemans, H. Ruhl, and T. Cowan, in *Advanced Accelerator Concepts*, edited by M. Conde and C. Eyberger (Amer. Inst. Phys., New York, 2006), vol. 877, pp. 213–219.

[45] H. Ruhl, *Collective Super-Intense Laser-Plasma Interactions*, Habilitationsschrift, Technischen Universität Darmstadt (2000).

[46] T. Z. Esirkepov, Comput. Phys. Commun. **135**, 144 (2001).

[47] W. B. Mori, (private communication).

[48] E. Michel, (in preparation).